pathoDISCO-HE: Towards light sheet microscopy enabled volumetric histopathology of human gliomas

James Oakes-Klein

james.oakes@tuwien.ac.at

Vienna University of Technology

Saiedeh Saghafi

Vienna University of Technology

Thomas Roetzer-Pejrimovsky

Medical University of Vienna

Christoph Fuchssteiner

Medical University of Vienna

Katherina Grin

Medical University of Vienna

Barbara Kiesel

Medical University of Vienna

Lisa Körner

Medical University of Vienna

Adelheid Wöhrer

Medical University of Vienna

Georg Widhalm

Medical University of Vienna

Hans-Ulrich Dodt

Vienna University of Technology

Research Article

Keywords: tissue clearing, cancer, tumour, light sheet, microscopy, histology, glioma, glioblastoma, histopathology

Posted Date: February 19th, 2025

DOI: https://doi.org/10.21203/rs.3.rs-5996603/v1

Additional Declarations: Competing interest reported. HUD has filed a patent for a 3D pathology method (WO2020002251A1). HUD and SS have filed a patent relating to the optical system used in this study (DE112014003369A5).

Abstract

Histopathological assessment of human tumours relies heavily upon traditional slide-based techniques such as H&E staining and immunohistochemistry. Whilst providing excellent resolution, traditional histological techniques require destruction of the specimen and do not provide details of three-dimensional tissue architecture. Glioblastomas are amongst the most spatially heterogeneous of human tumours, making them a prime target for the growing field of volumetric histopathology.

Tissue clearing and light sheet microscopy are complementary technologies allowing high-resolution volumetric imaging of biological specimens. In this study we aimed to explore the possibility of using these techniques as tools for volumetric histopathology of human gliomas. Starting with the previously published pathoDISCO protocol, we added pigment bleaching and fluorescent nuclear labelling stages to develop a protocol capable of clearing glioma specimens up to several millimetres thick within a few days. Using cresyl violet as a nuclear label and autofluorescence as an eosin analogue we were able to produce realistic “virtual H&E” images using a simple image post-processing pipeline. Virtual H&E images accurately represented several key pathological features of gliomas including necrosis, hypercellularity, microvascular proliferations and glomeruloid and garland vascular structures. The virtual H&E images can be viewed three dimensionally with only limited loss of resolution in z-projections. The volumetric imaging data could also be visualised by maximum intensity projection, allowing tracing of vascular structures throughout the tissue and identification of discrete zones of differing cellular or vascular density. Finally, we showed that our virtual H&E protocol is reversible and post-hoc traditional histology can be applied if necessary.

Overall, our study represents a novel contribution to the palette of volumetric histopathology techniques which may eventually allow more accurate and detailed characterisation of human tumours, thus facilitating more accurate diagnosis and prognosis and selection of the most effective personalised therapies, potentially improving patient outcomes.

Introduction

Malignant primary brain tumours affect 7 in 100000 people per year and 80–85% are gliomas (Schaff and Mellinghoff 2023). Gliomas arise from the many types of glial cells, meaning that there is also a diverse range of glioma types including astrocytomas, oligodendrogliomas and others. Glioma classification is based on the *WHO Classification of Tumours of the CNS* (Louis et al. 2021). Less aggressive tumours are graded 1 or 2 (low grade) whereas more aggressive tumours are graded 3 or 4 (high grade). High-grade gliomas are associated with poor prognosis and include astrocytoma (grade 3 or 4), oligodendroglioma (grade 3 and glioblastoma (grade 4) (Wang et al. 2023).

Imaging of gliomas *in situ* is performed predominately by using magnetic resonance imaging. This imaging provides information relating to the size and location of the lesion and first estimations if the glioma is low-grade or high-grade. Following neurosurgical biopsy or surgical resection tumours are classified using specific histopathological and molecular techniques (Perry and Wesseling 2016).

Histopathological analysis of tumours relies on laborious mechanical sectioning of samples and haematoxylin and eosin staining. Whilst this technique provides excellent resolution, there are also several drawbacks, including scoring or destruction of sections. In addition, traditional techniques are limited by a vast under-sampling factor. For example, sectioning of a 1cm thick tumour specimen at 5μm would result in production of 2000 sections; realistically, only a small number of these are examined, meaning that important histological features may be missed. This may present a particular problem for accurate characterisation of glioblastomas which can be spatially heterogenous even within a single lesion (Wang et al. 2023).

The field of tissue clearing is concerned with transforming a tissue specimen from its opaque native state to a state of optical transparency, primarily to allow examination using optical sectioning microscopy techniques such as light sheet microscopy (selective plane illumination microscopy) and confocal microscopy, usually combined with fluorescent labelling. This is a promising emerging technique for digital histological characterisation of intact tumour specimens. This approach overcomes the problems associated with traditional histology techniques as specimens can be processed without sectioning; instead, optical sections are collected by light sheet microscopy. This approach has the added benefit that specimens can be prepared rapidly and 100s-1000s of optical sections can be produced and analysed quickly (Sabdyusheva Litschauer et al. 2020). Previous studies have presented techniques for clearing and virtual histopathology of several different pathologies, including prostate, bladder, ovarian and breast cancers, lymphoma and lung amyloidosis (Glaser et al. 2017; Nojima et al. 2017; Reder et al. 2019; Tanaka et al. 2018; Tanaka et al. 2017).

Hydrophilic CUBIC clearing, fluorescent labelling and 3D microscopy techniques allowed imaging of various pathologies, allowing identification of nuclear atypia in lymphoma specimens and amyloid deposits in lung amyloidosis. Perhaps most importantly, this study demonstrated that a combination of 3D histopathology and traditional sectioning-based techniques was more sensitive at detecting metastatic colorectal adenocarcinoma nodules in lymph nodes than traditional sectioning-based techniques alone. This finding is very important for the emerging field of 3D histopathology, as it confirms that the technique can improve diagnosis and in turn is likely to be beneficial in terms of patient outcomes (Nojima et al. 2017).

The hydrogel embedding CLARITY protocol was used to clear prostate core needle biopsies; the specimens were stained with the fluorescent nuclear label DRAQ5 and eosin and imaged on an open-top light sheet microscopy system. The resulting data was processed to produce images similar to standard haematoxylin and eosin preparations, allowing histopathological evaluation (Glaser et al. 2017). A benefit of this “virtual haematoxylin and eosin” approach is that the resulting images can be analysed by any neuropathologist, not necessarily by a specialist in fluorescence microscopy data.

Some progress has already been made towards characterisation of brain tumours using tissue clearing and 3D microscopy techniques. Combination of iDISCO + and CUBIC tissue clearing with two-photon and confocal microscopy respectively allowed visualisation and morphological characterisation of some

brain tumour features. Immunolabelling was utilised to visualise astrocytes (GFAP) in glioblastoma specimens, whereas SOX2, CD31 and CD45 were used to characterise stemness, microvascular proliferation and immune infiltration respectively (Xu et al. 2023; Yang et al. 2020).

Whilst surface imaging by light sheet microscopy without tissue clearing is a possibility (Gao et al. 2023), for imaging the entirety of large specimens it is absolutely essential that a robust tissue clearing method is employed. Our group recently published the first method (pathoDISCO) for rapid, active dehydration of tumour samples (Sabdyusheva Litschauer et al. 2020). Instead of relying on passive diffusion for dehydration, this technique employs the water scavenging compound 2,2-dimethoxypropane (DMP) which actively reacts with water to produce methanol and acetone, resulting in extremely rapid dehydration.

The original pathoDISCO technique relies on imaging of autofluorescence. This method produced samples adequately clear for high-resolution light sheet microscopy and subsequent visualisation allowed identification of a range of characteristic breast tumour features. However, there are several limitations to this technique. For example, due to the non-specific nature of autofluorescence imaging, visualisation tends to be somewhat monochromatic and lacks the contrast observed with standard histopathological techniques. In addition to this, histopathologists are unlikely to be accustomed to reviewing tumour morphology visualised by autofluorescence imaging alone; a significant barrier to introducing the technique to the clinic (Sabdyusheva Litschauer et al. 2020).

In this article, we report the development of an improved method for 3D histopathology utilising rapid tissue dehydration. In this method, called pathoDISCO-HE, we combine rapid tissue clearing of glioma specimens and fluorescent labelling of nuclei. Following lightsheet microscopy imaging we applied a colour channel combining algorithm to produce virtual H&E sections with similar colours and hues as traditional haematoxylin and eosin staining. Virtual H&E processed image stacks can be viewed volumetrically from any angle, with only limited loss of resolution in z-projections. Volumetric data can also be rendered by maximum intensity projection, allowing visualisation of spatial heterogeneity of vascular structures and nuclei distribution.

Overall, this technique builds upon previous studies working towards realising the use of 3D histopathology techniques in clinical settings. pathoDISCO-HE can clear larger tumour specimens more quickly than previous techniques and this is important in 3D histopathology field.

Methods

Sample collection and ethical approval

In the present study, tumor samples from resection of newly diagnosed or recurrent suspected diffusely infiltrating gliomas (CNS WHO grades 2–4) were collected at the Department for Neurosurgery, Medical University of Vienna. After sufficient material for routine neuropathological analyses had been collected, residual tumor samples were formalin fixed and immediately transferred for further work-up to the

Center for Brain Research, Medical University of Vienna. The histopathological diagnosis of each included tumor was made by the local neuropathology team according to the latest WHO classification (5th edition, 2021). A detailed list of included tumor diagnoses is provided in Table 1. The study was approved by the ethics committee of the Medical University of Vienna.

Sample preparation, staining and rapid tissue clearing

Collected samples were bleached using a strategy similar to the previously published iDISCO protocol (Renier et al. 2014). Following brief washing in PBS, samples were dehydrated in a methanol/PBS gradient (0%, 0%, 50%, 70%, 90%, 100%, 100%, room temperature, 1hr per step) before bleaching in 2–5% H_2O_2 in methanol at 4°C overnight (methanol: Sigma-Aldrich, 32213; Dulbecco's PBS: 2.68mM KCl, 1.47mM KH_2PO_4, 428 136.89mM NaCl, 8.10mM Na_2HPO_4, pH7.4; H_2O_2: Carl Roth, 0034). Afterwards, samples were rehydrated in methanol-PBS gradient (reverse of above). The necessity of bleaching depends on the pigmentation of the sample, bleaching can be entirely omitted for samples which appear lightly or non-pigmented (as non-pathological brain tissue) whereas 5% H_2O_2 is required for more heavily pigmented samples. For a standard protocol 5% H_2O_2 is recommended as this gives the best bleaching effect and does not seem to negatively affect the integrity of the specimen.

Then, samples were stained with cresyl violet (Carl Roth, 7651) diluted 1:50 in 5% CHAPS/PBS (CHAPS: Hopax Fine Chemicals) overnight at room temperature (cresyl violet stock: 1mg/ml in dH_2O). Following washing in PBS (2x1hr, room temperature) samples were dehydrated for the final time. This protocol utilises active dehydration by the ketal 2,2-dimethoxypropane (DMP) (Sigma-Aldrich, D136808) which reacts with water to produce methanol and acetone (Sabdyusheva Litschauer et al. 2020; Stern and Dorer 1962). The reaction of ketals with water requires an acid catalyst, samples were acidified with HCl pH1 in dH_2O for 1hr at room temperature. Subsequently, samples were dehydrated using 2,2-dimethoxypropane (DMP), a further 25µl of 2N HCl was added per 5ml of DMP used. Samples were incubated in DMP for 2x30mins at 37°C. Finally, refractive index matching was performed by immersing the dehydrated samples in dibenzyl ether (DBE) (Sigma-Aldrich, 108014). All clearing stages were performed with moderate shaking.

Light sheet microscopy

Following refractive index matching, samples were mounted in a vascular clamp in an optical glass cuvette filled with DBE. This study used a previously described custom light sheet microscope. For light sheet generation we utilised an optical system developed as a continuation of our previous work with a modified optical design to produce a light sheet with optimised characteristics (Foroughipour et al. 2024; Saghafi et al. 2022; Saghafi et al. 2014; Saghafi et al. 2010; Saghafi et al. 2018). In the most recent version of this system the mirror system has been replaced with fibre optics (Omicron, Germany) and an automated XY stage has been added (Thor Labs, USA). A refractive index corrected XLFluor-340 NA 0.28

4x objective (Zeiss, Germany) and a 16x Fluotar NA 0.6 immersion objective (Leica, Germany) were used for image acquisition. Cresyl violet fluorescence was captured using the 532nm illumination laser with a 620/52nm bandpass filter whereas autofluorescence was recorded using the 488nm laser with a 525/50nm bandpass filter.

Image processing and visualisation

Image post-processing, including deconvolution, stripe artifact removal and unsharp masking, was performed in NeuroDeblur (Becker et al. 2021) (MBF Bioscience, United States). Image manipulations such as rolling ball background subtraction, local contrast normalisation (Integral image filters plugin) and FFT bandpass filtering were performed in Fiji (Schindelin et al. 2012). Prior to virtual H&E staining, stacks were aligned using BigStitcher in Fiji (Hörl et al. 2019). Virtual H&E visualisation was performed in NeuroDeblur. A schematic for image post-processing is provided in Fig. 1C. 3D visualisation of light sheet data was performed using Amira 3D (v2023.1.1, Thermo Fisher Scientific).

Histological staining and immunohistochemistry

Subsequent to clearing and light sheet imaging, specimens #4–13 were rehydrated in a graded methanol series and washed in PBS. Specimens were processed and embedded in paraffin using standard techniques followed by microtome sectioning at 5µm. For H&E staining sections were dewaxed in xylene and rehydrated in a graded ethanol series before nuclear staining in Mayer's haematoxylin (Merck #1.09249). Sections were rinsed in tap water, differentiated in HCl-ethanol (70% ethanol + 0.5% v/v concentrated (37%) HCl) and blued in Scott's solution (dH_2O + 0.2% w/v $KHCO_3$ + 2% w/v $MgSO_4.7H_2O$). After further rinsing in tap water, sections were stained in aqueous eosin, dehydrated in a graded ethanol series, and cleared in n-butyl acetate. Sections were mounted with DPX. H&E stained slides were imaged on a Zeiss Axioplan compound microscope.

For IHC staining the following antibodies and dilutions were utilised: IDH1 R132H (1:25 Dianova #DIA-H09), CD34 (1:100 Novocastra #NCL-L-END), p53 (1:50, Dako #M7001), OLIG2 (1:1000 IBL #18953), Ki-67 / MIB-1 (1:200 Dako #M7240), GFAP (1:3000 Dako #Z0334). IHC staining was performed on a Dako Autostainer PlusLink (CD34, p53, OLIG2, Ki-67, GFAP) or Ventana Benchmark Autostainer (IDH1 R132H).

For Klüver-Barrera staining sections were dewaxed in xylene and rehydrated to 95% ethanol. Sections were incubated in luxol fast blue solution (0.1% w/v in 95% ethanol) at 60°C overnight. After cooling, sections were fully rehydrated and differentiated in 0.05% w/v lithium carbonate. Sections were then stained with cresyl violet (0.1%w/v in dH_2O + 20 drops of 10% acetic acid) for 5-10mins at 60°C. Sections were differentiated in 95% ethanol, dehydrated twice in 100% ethanol and cleared in xylene. Sections were mounted using Entellan New (Merck #1.07961) and imaged on an Olympus VS ASW S6 slide scanning microscope.

Table 1
Summary of glioma specimens utilised in this study.

Sample ID	Diagnosis	CNS WHO grade	IDH status
#01	Glioblastoma (recurrent)	4	Wild type
#02	Glioblastoma	4	Wild type
#03	Glioblastoma	4	Wild type
#04	Glioblastoma	4	Wild type
#05	Glioblastoma (recurrent)	4	Wild type
#06	Glioblastoma	4	Wild type
#07	Glioblastoma (recurrent)	4	Wild type
#08	Astrocytoma (recurrent)	3	Mutant
#09	Astrocytoma	4	Mutant
#10	Glioblastoma	4	Wild type
#11	Astrocytoma (recurrent)*	2	Mutant
#12	Glioblastoma (recurrent)	4	Wild type
#13	Glioblastoma	4	Wild type

*#11 contained mainly gliosis, tumour cells only rarely observed.

Results

Development of pathoDISCO-HE

The pathoDISCO-HE protocol combines aspects of the original pathoDISCO protocol and the iDISCO protocol (Renier et al. 2014; Sabdyusheva Litschauer et al. 2020). Initial experimentation revealed that glioblastoma specimens could not be adequately cleared by the original pathoDISCO protocol, which was optimised for clearing of breast tumour tissues. In our experience, glioblastoma specimens exhibited darker pigmentation than breast tumour specimens and as such we reasoned that addition of a bleaching or decolourisation procedure could be necessary. This led us to the addition of a hydrogen peroxide bleaching stage performed immediately after fixation of the tissue. This bleaching stage was performed in a similar way to the iDISCO protocol; this involves dehydrating the tissue in a methanol gradient and bleaching using a solution consisting of hydrogen peroxide diluted in methanol (Renier et al. 2014). With addition of the bleaching stage we were able to clear specimens up to a thickness of several millimetres (Fig. 1).

In order to facilitate virtual H&E labelling by fluorescence microscopy it was essential to find a fluorescent nuclear label effective in glioblastoma tissue and compatible with our clearing protocol. We found cresyl violet, well-known to neurobiologists as a fluorescent Nissl stain, to be an adequate nuclear label in glioblastoma specimens (Alvarez-Buylla et al. 1990) (Fig. 1). Although usually performing excellently, occasional problems were encountered; for example, larger specimens sometimes exhibited incomplete dye penetration and highly dense samples were sometimes over-stained, reducing the quality of light sheet imaging. Measurement of the maximum imaging depth at which nuclei could still be visualised across the field of view in all recordings revealed a median maximum depth of 755µm (range: 153–2082µm, n = 27). Analysis of light sheet images from specimens which were incompletely labelled allowed us to determine that the median penetration depth of cresyl violet was 522µm (range: 240–802µm, n = 9). The stain penetration and possible imaging depth is dependent on various parameters including specimen size and structure, depigmentation efficiency and cellular density.

Cleared and stained specimens were imaged by light sheet microscopy and images post-processed using a straightforward pipeline (Fig. 1). Samples were imaged using two illumination and emission wavelength combinations. Cresyl violet fluorescence was imaged using a 532nm excitation laser combined with a 620/52nm bandpass emission filter. Autofluorescence was used as an eosin analogue and was recorded using a 488nm excitation laser combined with a 525/50nm bandpass emission filter. The resulting stacks were subsequently post-processed using NeuroDeblur (MBF Biosciences) and Fiji (Hörl et al. 2019; Schindelin et al. 2012). Nuclear segmentation was performed using rolling ball background subtraction, achieving adequate results in most cases. Some specimens exhibited a comparatively poor signal-to-noise ratio in the nuclear labelling channel, and nuclear segmentation by rolling ball background subtraction was found to be ineffective. Instead, these poor signal-to-noise ratio specimens were subjected to local contrast normalisation and FFT bandpass filtering, this approach yielded acceptable nuclear segmentation but with a qualitatively reduced resolution. A schematic of the image processing pipeline employed in this study is provided in Fig. 1C.

Following image post-processing, the grayscale images were used to produce virtual H&E stained optical sections. NeuroDeblur includes a “colour channel combiner” plugin which can perform additive or subtractive colour mixing, in this study the “virtual-HE staining” preset was utilised. The graphical interface allows the user to load nuclear and cytoplasm stacks, apply intensity thresholds, and adjust RGB colour and colour balance (Fig. 1D). This approach allowed us to process light sheet fluorescence microscopy images to mimic staining produced by standard histological techniques.

pathoDISCO-HE allows identification of characteristic histological features of gliomas

In order to test our pathoDISCO-HE protocol we processed residual specimens from a number of patients, mainly with glioblastoma diagnoses, but also from two patients with grade 2 and grade 3

astrocytomas (Table 1). Application of the protocol to glioblastoma specimens and subsequent virtual H&E visualisation allowed identification of many characteristic features (Fig. 2).

Nuclear labelling with cresyl violet allowed observation of nuclear density which ranged from relatively sparse (Fig. 2F **+ J**) to highly dense (Fig. 2H,I,S). Varying cell types and nuclear morphology could be observed, with nuclei varying widely in size and shape. Cells with a neuronal morphology could be occasionally observed (Fig. 2E,F,N,P). In some samples, especially when a low magnification objective with a wide field-of-view was utilised, the infiltrating border could be visualised (Fig. 2G **+ M**). When using a high magnification objective nuclear chromatin structure could be observed (Fig. 2D). One specimen exhibited a characteristic spindle cell appearance (Fig. 2H).

Gliomas are frequently accompanied by various characteristic vascular features. Information relating to tumour vasculature was provided by the autofluorescence channel, used as an eosin analogue. The most frequently observed vascular transformation was microvascular proliferation (Fig. 2A,C,G,M,Q). Glomeruloid and garland-like vascular structures were only observed in one specimen each (Fig. 2Q,R,W). Additional pathological features such as necrosis (Fig. 2A,C,U) and microcystic spaces (Fig. 2J **+ O**) were also observed. Example virtual H&E images from each processed specimen are provided in **Additional File 1**.

Volumetric histopathology by 3D visualisation of light sheet microscopy data

Following image post-processing and virtual H&E rendering, we assessed the suitability of our data sets for 3D visualisation (Fig. 3). The ability to view data in three dimensions is a major benefit of our approach, as it allows the specimen to be viewed from any angle or at any depth. In addition, some features such as vascular morphology cannot be easily assessed in standard two-dimensional histopathology. Data from each specimen was loaded into Amira 3D (Thermo Fisher Scientific), both as virtual H&E processed RGB images and as individual grayscale channels. The greyscale channels representing autofluorescence and cresyl violet staining were assigned green and red colourmaps respectively and visualised using maximum intensity projection.

3D rendering of virtual H&E processed images allowed rapid inspection of the intact specimen by zooming through the XY and Z planes. Specimens often exhibited comparable or only slightly reduced resolution in the Z-planes compared to XY plane (Fig. 3H,J,L,F,G,Q,R,U), however this was occasionally significantly lower (**Additional file 1**).

Blood vessels exhibit high levels of autofluorescence, allowing visualisation of the varied vascular structures present in glioblastoma specimens. This approach allowed identification of two distinct vascular signatures within a single glioblastoma specimen, namely garland vascular structures and an adjacent network of less densely packed vessels (Fig. 3C). Elongated endothelial nuclei could be seen bordering the garland structures, which were also surrounded by highly dense tumour cells (Fig. 3D **+ D'**).

In another glioblastoma specimen a glomeruloid vessel could be traced over several millimetres (Fig. 3E). The histological morphology of the glomeruloid vessel could be viewed in all axes with good resolution by virtual H&E rendering (Fig. 3F **+ G**). Several glioblastoma specimens exhibited large vascular structures exhibiting high autofluorescence (Fig. 3I,K,M,V).

Examination of 20µm thick virtual slices through the glioblastoma specimens allowed visualisation of sub-cellular structures such as neurites and chromatin (Fig. 3N,N**',O,O'**). The same approach allowed identification of discrete cellular zones comprising small nucleated tumour cells and larger cells of neuronal morphology (Fig. 3P). In the neuronal-type cells cresyl violet signal overlapped somewhat with the autofluorescent signal, presumably due to accumulation of autofluorescent lipofuscins in the neuronal cell bodies (Chang et al. 2023; Goyal 1982; Pesce et al. 2022). A similar observation was made in another sample, however with highly discrete zones of cellular density rather than cell type (Fig. 3T). Further examples of 3D visualisation are provided in **Additional file 1** and **Supplementary videos 1–6**.

pathoDISCO-HE is reversible and compatible with post-hoc standard histology and immunohistochemistry

Following pathoDISCO-HE processing, specimens were re-processed using standard histology techniques and H&E staining to produce correlative images (Fig. 4). Stained sections appeared normal and did not significantly differ from specimens not previously subjected to pathoDISCO-HE processing. This result demonstrates that post-hoc standard histology can be performed following pathoDISCO-HE processing if required. Re-processing previously cleared and imaged specimens also allowed us to make a direct comparison of image quality in the two techniques. As expected, the resolution achieved in standard histology was slightly better than that observed using light sheet microscopy. In particular the hues of eosin staining were not always exactly recapitulated by light sheet autofluorescence imaging. However, the main benefit of light sheet enabled volumetric histology over standard histology is the ability to image an intact specimen and visualise it in three-dimensions. Although this benefit comes at a slight cost in terms of resolution, a plethora of pathological features are accurately recapitulated in virtual-H&E processed images. In particular, glomeruloid vascular structures are easily identifiable (Fig. 4E), as are microcystic spaces (Fig. 4A **+ H**) and hypercellular regions (Fig. 4B **+ G**). Some specimens, presumably from the tumour margin, contained both small glioma cells and cells with neuronal morphology; these cell types could easily be distinguished in virtual H&E images (**Figure C + F**).

Immunohistochemistry forms a crucial part of modern histopathological profiling. We tested the compatibility of our protocol with *post hoc* immunolabelling with a panel of glioma relevant antibodies comprising the tumour suppressor p53, the oligodendrocyte marker OLIG2, proliferation marker Ki-67, the astrocyte marker GFAP, mutant IDH1 protein (p.R132H), and the endothelial marker CD34 (Fig. 5A-F). In addition, we performed myelin staining by the Klüver-Barrera method – which may be performed if demyelinating disease is suspected (Fig. 5G-H). IHC staining performed mainly as would be expected, however the nuclear staining with Ki-67 and OLIG2 were slightly fainter than usual. These results

demonstrate compatibility of pathoDISCO-HE enabled 3D histopathology with subsequent immunolabelling.

Discussion

In this study we explored the possibilities of using tissue clearing and light sheet microscopy as tools for volumetric histopathology of gliomas. We developed a novel protocol capable of clearing and fluorescently labelling nuclei in glioma specimens. This was followed by light sheet microscopy to recorded autofluorescence and nuclear fluorescence, and eventually production of virtual H&E reconstructions.

The pathoDISCO-HE protocol draws upon elements of several established tissue clearing protocols. An iDISCO-style hydrogen peroxide bleaching stage (Renier et al. 2014) is followed by nuclear labelling with cresyl violet. To facilitate rapid penetration of cresyl violet deep into glioma specimens we opted to combine to cresyl violet stain with CHAPS detergent. CHAPS is a zwitterionic detergent with superior membrane permeabilising activity in comparison to other commonly used detergents (Zhao et al. 2020). Following fluorescent nuclear labelling by cresyl violet we dehydrated the specimens chemically by use of the compound 2,2-dimethoxypropane (DMP). DMP is a ketal, and therefore reacts with water in acidic conditions, to produce methanol and acetone. This reaction is highly efficient and allows extremely efficient specimen dehydration (Stern and Dorer 1962), especially compared to other hydrophobic clearing protocols which rely on diffusion of solvents for tissue dehydration. Use of DMP allowed us to dehydrate specimens of up to several millimetres in thickness in just one hour. Finally, dehydrated specimens were incubated in dibenzyl ether for refractive index matching. In total, our protocol requires around four days from receiving a formalin fixed tissue specimen to production of a 3D reconstruction. This is significantly quicker than previous clearing protocols for human brain tumours; for example CUBIC and iDISCO + processing required around 1.5-3 weeks. However, these studies did additionally employ immunolabelling, which requires longer incubation than labelling with small fluorescent molecules such as cresyl violet (Xu et al. 2023; Yang et al. 2020).

pathoDISCO-HE allowed visualisation of nuclei across the whole field of view down to a median depth of 755µm (range: 153–2082µm, n = 27), though nuclear labelling at the periphery of specimens was usually visible at much greater depths. Measurement of stain penetration in incompletely labelled slices revealed a median penetration depth of 522µm (range: 240–802µm, n = 9). It is worth noting that vasculature could often be visualised at much greater depths than nuclear labelling, as autofluorescence is not dependent on penetration of a fluorescent label. Stain penetration could be improved by stronger membrane permeabilising treatments and longer incubation in the staining solution. The maximum imaging depth is also influenced by a number of factors, but is primarily reliant on the quality of the clearing procedure and excitation and emission wavelengths employed. In our experience gliomas are a difficult tissue to work with due to the often extremely high cell density and extensive vasculature. Sub-optimally cleared specimens exhibit lower maximum imaging depths due to scattering of both the illumination light sheet and emitted fluorescence. Future improvements to the method could include

improved clearing efficiency and use of fluorescent labels with excitation and emission wavelengths in the far red or near infrared range, as higher wavelengths are significantly less scattered by biological tissues (Jacques 2013).

pathoDISCO-HE processed specimens yielded images reminiscent of traditional H&E preparations. However, some factors need to be considered when interpreting these images. For example, larger specimens occasionally exhibited incomplete penetration of the nuclear label. This could give the impression that nuclei are absent from some regions – it will be important to distinguish if this is due to incomplete stain penetration or a pathological hallmark such as necrosis. Stain penetration could be improved by using a more efficient tissue permeabilisation treatment or by longer incubation in the staining solution.

Whilst most features of traditional H&E sections were accurately represented by pathoDISCO-HE, it was apparent that the variety of hues imparted onto sections by eosin staining was less extensive in virtually stained images. In the present study we did not employ any specific stain to mimic eosin staining, instead opting to use autofluorescence imaging. An improved virtual H&E algorithm or application of a robust fluorescent cytoplasm label could improve the appearance of cytoplasm in virtual H&E images in future studies. Occasionally, when using the normalisation + bandpass filter method for nuclear segmentation, some background signal was observed in the virtual HE nuclei channel, this could also be corrected by improvements to the post-processing methods.

Light sheet microscopy is just one of a number of available volumetric optical imaging techniques. In addition to light sheet microscopy, techniques including confocal microscopy and two-photon microscopy also show promise as tools for 3D histopathology.

Confocal microscopy is a fluorescence microscopy technique which achieves optical sectioning by spatial filtering of out-of-focus light. Although confocal microscopy can provide higher lateral resolution than light sheet microscopy, the imaging depth in generally limited to 100's of μm. Confocal microscopy has been applied to cleared tumour tissue in a number of previous studies. CUBIC cleared lymph nodes from malignant lymphoma were imaged by confocal microscopy, allowing characterisation of nuclear characteristics such as atypia and pleomorphism (Nojima et al. 2017).

Two-photon microscopy allows greater penetration of excitation lasers into tissue due to the use of higher wavelengths, typically in the near-infrared range. These systems take advantage of the two photon effect, whereby fluorophores are excited by two-photons simultaneously. Two-photon microscopy was used to image immunolabelled brain tumour specimens, revealing significant spatial heterogeneity (Yang et al. 2020). Two-photon lasers are typically used in upright microscopes with episcopic illumination, however a two-photon light sheet microscope has been developed for imaging of human tumours. This system was used to perform rapid imaging of uncleared nuclear labelled human skin, pancreatic and prostatic cancers. Nuclear labelling allowed production of virtual H&E images however the imaging depth was limited to < 100μm, probably due to scattering of emitted fluorescence (Park et al. 2024).

Recently, stimulated Raman histology (SRH) has been introduced to produce two-dimensional virtual H&E images intraoperatively. This technique is extremely fast, giving the neurosurgeon almost immediate feedback. Histological brain tumor diagnoses established by SRH were extremely accurate, matching the final histopathological diagnosis in 99% of cases (Wadiura et al. 2022).

Within the landscape of optical imaging techniques for histological characterisation of tumour specimens, light sheet microscopy occupies a unique position in terms of high resolution and the ability to image large intact specimens. A disadvantage is the relatively slow clearing process; in our protocol the clearing takes around two and a half days and the imaging and post-processing takes a further day. Although this pipeline could be significantly automated and streamlined for largescale applications, the pathoDISCO-HE method is best suited for further development as a technique to be performed alongside traditional slide based histopathology, rather than an intraoperative technique.

In addition to H&E staining the standard histological investigation of glioma specimens often also includes immunohistochemistry with primary antibodies against proteins such as mutant IDH1 (p.R132H), ATRX, p53, EGFR, Ki-67, pHH3 and CD34. We have demonstrated that pathoDISCO-HE is compatible with *post hoc* immunohistochemical labelling in 5µm sections (Fig. 5). The compatibility of whole mount immunofluorescence labelling with the pathoDISCO-HE protocol is yet to be investigated, however this is possible in some other techniques. For example, labelling of human brain tumours with various antibodies was achieved using the iDISCO + clearing protocol, yielding detailed information relating to the spatial heterogeneity of tumour cell differentiation and stemness (GFAP, SOX2), microvascular proliferation (CD31) and immune microenvironment (CD45) (Yang et al. 2020). We have utilised autofluorescence and cresyl violet fluorescence for cytoplasm and nuclear imaging. Autofluorescence was recorded in the green range (525/50 bandpass filter) whereas cresyl violet fluorescence was recorded in the red range (620/52nm bandpass filter). This leaves a considerable portion of the usable light spectrum which could be used for imaging of immunofluorescently labelled proteins as fluorophores are commonly available with emission wavelengths up to at least 800nm.

Historically, central nervous system tumours were classified based solely on their histological appearance. However, since 2016 the WHO classification system includes integrated diagnoses combining histology and molecular genetics, providing improved prognostic accuracy and treatment strategy selection (Ferris et al. 2017). Common molecular pathology investigations for gliomas include DNA sequencing to determine *IDH1/2* and *TERT* genotype, chromosomal alterations such as 1p/19q co-deletion and homozygous deletion of *CDKN2A/B*. *MGMT* methylation status may be determined using techniques such as bisulphite sequencing. Combination of molecular and histological diagnostic techniques results in a significant improvement in prognostic accuracy (Ferris et al. 2017). The starting point for these molecular investigations is the isolation of DNA. DNA should be well preserved in cleared tissue meaning that it can be extracted after the necessary imaging has been performed, yielding a fully integrated histological and molecular profile of the specimen.

The application of automated image analysis algorithms and artificial intelligence approaches to human cancer pathology is a rapidly expanding field of research. Tumour vasculature and angiogenesis has been a major target of volumetric microscopy techniques in recent years, both in mouse models and patient derived tissue (Baker et al. 2014; Breckwoldt et al. 2016; Cribaro et al. 2021; Lagerweij et al. 2017). Application of tissue clearing and light sheet microscopy to anti-CD34 immunolabelled urothelial carcinoma vasculature allowed calculation of various vascular parameters such as density, radius, tortuosity and kurtosis and association of these parameters with disease stage and muscle-invasive disease, thus demonstrating potential diagnostic applications (Tanaka et al. 2017). As discussed previously, molecular diagnostics are now extremely important for predicting patient prognosis and determining personalised treatments. A recent study utilising artificial intelligence based molecular classification was able to predict certain molecular alterations in glioblastomas from stimulated Raman histology with high accuracy, including *IDH* mutations, 1p19q co-deletion and *ATRX* mutation (Hollon et al. 2023). Such artificial intelligence based pattern recognition approaches may be applied to pathoDISCO-HE data in future studies, possibly allowing improved prognostic abilities, or allowing assessment of spatial heterogeneity not only in histological terms, but also in terms of molecular background.

Future implementation of volumetric histopathology techniques in clinical practice may result in enormous benefits for patients. Volumetric histopathology, in combination with molecular diagnostics and potentially AI-based analytical methods, would allow detailed and accurate characterisation of the entire specimen. This may allow clinicians to utilise a personalised medicine approach to accurately select the most appropriate treatments, thereby improving patient prognoses.

In summary, we have established a novel clearing and fluorescent nuclear labelling method allowing high resolution volumetric histopathological examination of human glioma specimens. Future work may achieve additional labelling with multiple antibodies, allowing enhanced analysis of tumour spatial heterogeneity. Implementation of automated image analysis algorithms quantifying cell density and vasculature parameters should be feasible, providing information which simply cannot be determined using traditional two-dimensional techniques. Overall, our work represents a contribution to the field of volumetric histopathology, a research field which may eventually allow more accurate diagnoses and prognoses, resulting in more efficient and personalised treatments for glioma patients.

Declarations

Ethics approval and consent to participate

The study was approved by the ethics committee of the Medical University of Vienna.

Consent for publication

All authors have approved the manuscript and consent to its publication.

Competing interests

HUD has filed a patent for a 3D pathology method (WO2020002251A1). HUD and SS have filed a patent relating to the optical system used in this study (DE112014003369A5).

Funding

This study was funded by the Austrian Science Fund (FWF) projects P31263 and P35614 and the German BMBF project 3Dpatho.

Acknowledgements

Not applicable.

Author contributions

Project was initiated by HUD and GW and conceptualised by JO and HUD. JO developed the clearing and staining method with the help of HUD. JO prepared and imaged specimens, performed post-processing and data analysis and wrote the manuscript with guidance from HUD. SS designed the light sheet microscope and provided instruction on optimal usage. AW and TRP provided histopathology expertise. TRP and CF contributed to slide based histology and immunohistochemistry. GW, KG, BK and LK provided glioma specimens and neurosurgical expertise. All authors approved and contributed to preparation of the manuscript.

References

1. Alvarez-Buylla A, Ling CY, Kirn JR. 1990. Cresyl violet: A red fluorescent nissl stain. J Neurosci Methods. 33(2-3):129-133.
2. Baker GJ, Yadav VN, Motsch S, Koschmann C, Calinescu A-A, Mineharu Y, Camelo-Piragua SI, Orringer D, Bannykh S, Nichols WS et al. 2014. Mechanisms of glioma formation: Iterative perivascular glioma growth and invasion leads to tumor progression, vegf-independent vascularization, and resistance to antiangiogenic therapy. Neoplasia. 16(7):543-561.
3. Becker K, Saghafi S, Pende M, Hahn C, Dodt HU. 2021. Visualizing minute details in light-sheet and confocal microscopy data by combining 3d rolling ball filtering and deconvolution. J Biophotonics.e202100290.
4. Breckwoldt MO, Bode J, Kurz FT, Hoffmann A, Ochs K, Ott M, Deumelandt K, Krüwel T, Schwarz D, Fischer M et al. 2016. Correlated magnetic resonance imaging and ultramicroscopy (mr-um) is a tool kit to assess the dynamics of glioma angiogenesis. Elife. 5:e11712.
5. Chang S, Yang J, Novoseltseva A, Abdelhakeem A, Hyman M, Fu X, Li C, Chen SC, Augustinack JC, Magnain C et al. 2023. Multi-scale label-free human brain imaging with integrated serial sectioning polarization sensitive optical coherence tomography and two-photon microscopy. Adv Sci (Weinh). 10(35):e2303381.

6. Cribaro GP, Saavedra-López E, Romarate L, Mitxitorena I, Díaz LR, Casanova PV, Roig-Martínez M, Gallego JM, Perez-Vallés A, Barcia C. 2021. Three-dimensional vascular microenvironment landscape in human glioblastoma. Acta Neuropathologica Communications. 9(1):24.
7. Ferris SP, Hofmann JW, Solomon DA, Perry A. 2017. Characterization of gliomas: From morphology to molecules. Virchows Arch. 471(2):257-269.
8. Foroughipour SM, Becker K, Foroughipour M, Ghaffari Tabrizi-Wizsy N, Sarem N, Fuchssteiner C, Saghafi S. 2024. Converting a symmetrical gaussian beam into a thin tunable light sheet. 1(1):65-75.
9. Gao G, Miyasato D, Barner LA, Serafin R, Bishop KW, Xie W, Glaser AK, Rosenthal EL, True LD, Liu JTC. 2023. Comprehensive surface histology of fresh resection margins with rapid open-top light-sheet (otls) microscopy. IEEE Trans Biomed Eng. 70(7):2160-2171.
10. Glaser AK, Reder NP, Chen Y, McCarty EF, Yin C, Wei L, Wang Y, True LD, Liu JTC. 2017. Light-sheet microscopy for slide-free non-destructive pathology of large clinical specimens. Nature Biomedical Engineering. 1(7):0084.
11. Goyal VK. 1982. Lipofuscin pigment accumulation in human brain during aging. Exp Gerontol. 17(6):481-487.
12. Hollon T, Jiang C, Chowdury A, Nasir-Moin M, Kondepudi A, Aabedi A, Adapa A, Al-Holou W, Heth J, Sagher O et al. 2023. Artificial-intelligence-based molecular classification of diffuse gliomas using rapid, label-free optical imaging. Nature Medicine. 29(4):828-832.
13. Hörl D, Rojas Rusak F, Preusser F, Tillberg P, Randel N, Chhetri RK, Cardona A, Keller PJ, Harz H, Leonhardt H et al. 2019. Bigstitcher: Reconstructing high-resolution image datasets of cleared and expanded samples. Nature Methods. 16(9):870-874.
14. Jacques SL. 2013. Optical properties of biological tissues: A review. Phys Med Biol. 58(11):R37-61.
15. Lagerweij T, Dusoswa SA, Negrean A, Hendrikx EML, de Vries HE, Kole J, Garcia-Vallejo JJ, Mansvelder HD, Vandertop WP, Noske DP et al. 2017. Optical clearing and fluorescence deep-tissue imaging for 3d quantitative analysis of the brain tumor microenvironment. Angiogenesis. 20(4):533-546.
16. Louis DN, Perry A, Wesseling P, Brat DJ, Cree IA, Figarella-Branger D, Hawkins C, Ng HK, Pfister SM, Reifenberger G et al. 2021. The 2021 who classification of tumors of the central nervous system: A summary. Neuro Oncol. 23(8):1231-1251.
17. Nojima S, Susaki EA, Yoshida K, Takemoto H, Tsujimura N, Iijima S, Takachi K, Nakahara Y, Tahara S, Ohshima K et al. 2017. Cubic pathology: Three-dimensional imaging for pathological diagnosis. Sci Rep. 7(1):9269.
18. Park WY, Yun J, Shin J, Oh BH, Yoon G, Hong SM, Kim KH. 2024. Open-top bessel beam two-photon light sheet microscopy for three-dimensional pathology. Elife. 12.
19. Perry A, Wesseling P. 2016. Chapter 5 - histologic classification of gliomas. In: Berger MS, Weller M, editors. Handbook of clinical neurology. Elsevier. p. 71-95.
20. Pesce L, Laurino A, Scardigli M, Yang J, Boas DA, Hof PR, Destrieux C, Costantini I, Pavone FS. 2022. Exploring the human cerebral cortex using confocal microscopy. Prog Biophys Mol Biol. 168:3-9.

21. Reder NP, Glaser AK, McCarty EF, Chen Y, True LD, Liu JTC. 2019. Open-top light-sheet microscopy image atlas of prostate core needle biopsies. Arch Pathol Lab Med. 143(9):1069-1075.
22. Renier N, Wu Z, Simon David J, Yang J, Ariel P, Tessier-Lavigne M. 2014. Idisco: A simple, rapid method to immunolabel large tissue samples for volume imaging. Cell. 159(4):896-910.
23. Sabdyusheva Litschauer I, Becker K, Saghafi S, Ballke S, Bollwein C, Foroughipour M, Gaugeler J, Foroughipour M, Schavelová V, László V et al. 2020. 3d histopathology of human tumours by fast clearing and ultramicroscopy. Scientific Reports. 10(1):17619.
24. Saghafi S, Becker K, Gori F, Foroughipour M, Bollwein C, Foroughipour M, Steiger K, Weichert W, Dodt H-U. 2022. Engineering a better light sheet in an axicon-based system using a flattened gaussian beam of low order. Journal of Biophotonics. 15(6):e202100342.
25. Saghafi S, Becker K, Hahn C, Dodt HU. 2014. 3d-ultramicroscopy utilizing aspheric optics. J Biophotonics. 7(1-2):117-125.
26. Saghafi S, Becker K, Jährling N, Richter M, Kramer ER, Dodt H-U. 2010. Image enhancement in ultramicroscopy by improved laser light sheets. Journal of Biophotonics. 3(10-11):686-695.
27. Saghafi S, Haghi-Danaloo N, Becker K, Sabdyusheva I, Foroughipour M, Hahn C, Pende M, Wanis M, Bergmann M, Stift J et al. 2018. Reshaping a multimode laser beam into a constructed gaussian beam for generating a thin light sheet. J Biophotonics. 11(6):e201700213.
28. Schaff LR, Mellinghoff IK. 2023. Glioblastoma and other primary brain malignancies in adults: A review. Jama. 329(7):574-587.
29. Schindelin J, Arganda-Carreras I, Frise E, Kaynig V, Longair M, Pietzsch T, Preibisch S, Rueden C, Saalfeld S, Schmid B et al. 2012. Fiji: An open-source platform for biological-image analysis. Nature Methods. 9(7):676-682.
30. Stern JH, Dorer FH. 1962. Standard heats of formation of 2,2-dimethoxypropane (l), and 2,2-diethoxypropane (l). Group additivity theory and calculated heats of formation of five ketals. The Journal of Physical Chemistry. 66(1):97-99.
31. Tanaka N, Kaczynska D, Kanatani S, Sahlgren C, Mitura P, Stepulak A, Miyakawa A, Wiklund P, Uhlen P. 2018. Mapping of the three-dimensional lymphatic microvasculature in bladder tumours using light-sheet microscopy. Br J Cancer. 118(7):995-999.
32. Tanaka N, Kanatani S, Tomer R, Sahlgren C, Kronqvist P, Kaczynska D, Louhivuori L, Kis L, Lindh C, Mitura P et al. 2017. Whole-tissue biopsy phenotyping of three-dimensional tumours reveals patterns of cancer heterogeneity. Nat Biomed Eng. 1(10):796-806.
33. Wadiura LI, Kiesel B, Roetzer-Pejrimovsky T, Mischkulnig M, Vogel CC, Hainfellner JA, Matula C, Freudiger CW, Orringer DA, Wöhrer A et al. 2022. Toward digital histopathological assessment in surgery for central nervous system tumors using stimulated raman histology. Neurosurg Focus. 53(6):E12.
34. Wang LM, Englander ZK, Miller ML, Bruce JN. 2023. Malignant glioma. Adv Exp Med Biol. 1405:1-30.
35. Xu Y, He Q, Wang M, Wu Y, Shi Y, Wang W, Zhang J. 2023. Three-dimensional visualization of human brain tumors using the cubic technique. Brain Tumor Pathol. 40(1):4-14.

36. Yang R, Guo J, Lin Z, Song H, Feng Z, Ou Y, Zhou M, Li Y, Yi G, Li K et al. 2020. The combination of two-dimensional and three-dimensional analysis methods contributes to the understanding of glioblastoma spatial heterogeneity. J Biophotonics. 13(2):e201900196.
37. Zhao S, Todorov MI, Cai R, Maskari RAI, Steinke H, Kemter E, Mai H, Rong Z, Warmer M, Stanic K et al. 2020. Cellular and molecular probing of intact human organs. Cell. 180(4):796-812.e719.

Figures

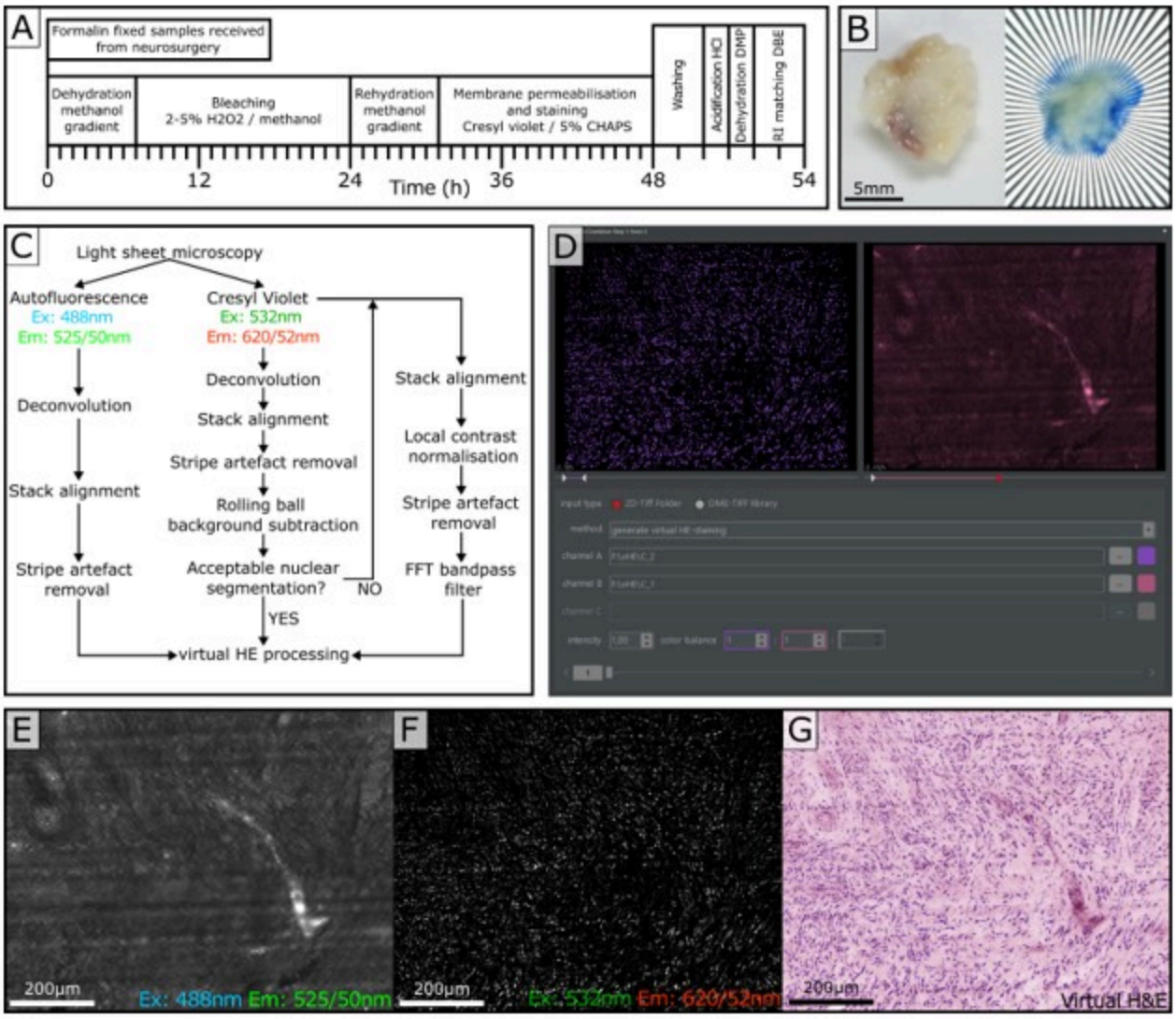

Figure 1

Clearing, labelling, imaging and post-processing strategy for glioma virtual histopathology. A: Procedure and timeline for pathoDISCO-HE sample processing. **B:** Glioblastoma specimen before and after processing, exhibiting good transparency after clearing. **C:** Procedure for data acquisition by light sheet microscopy and subsequent post-processing to produce virtual HE images. **D:** Colour channel combiner interface in NeuroDeblur. **E-G:** Example post-processed light sheet images and virtual H&E image from

glioblastoma specimen. **E:** Autofluorescence stack (eosin analogue). **F:** Cresyl violet stack (nuclear labelling). **G:** virtual H&E composite produced in NeuroDeblur.

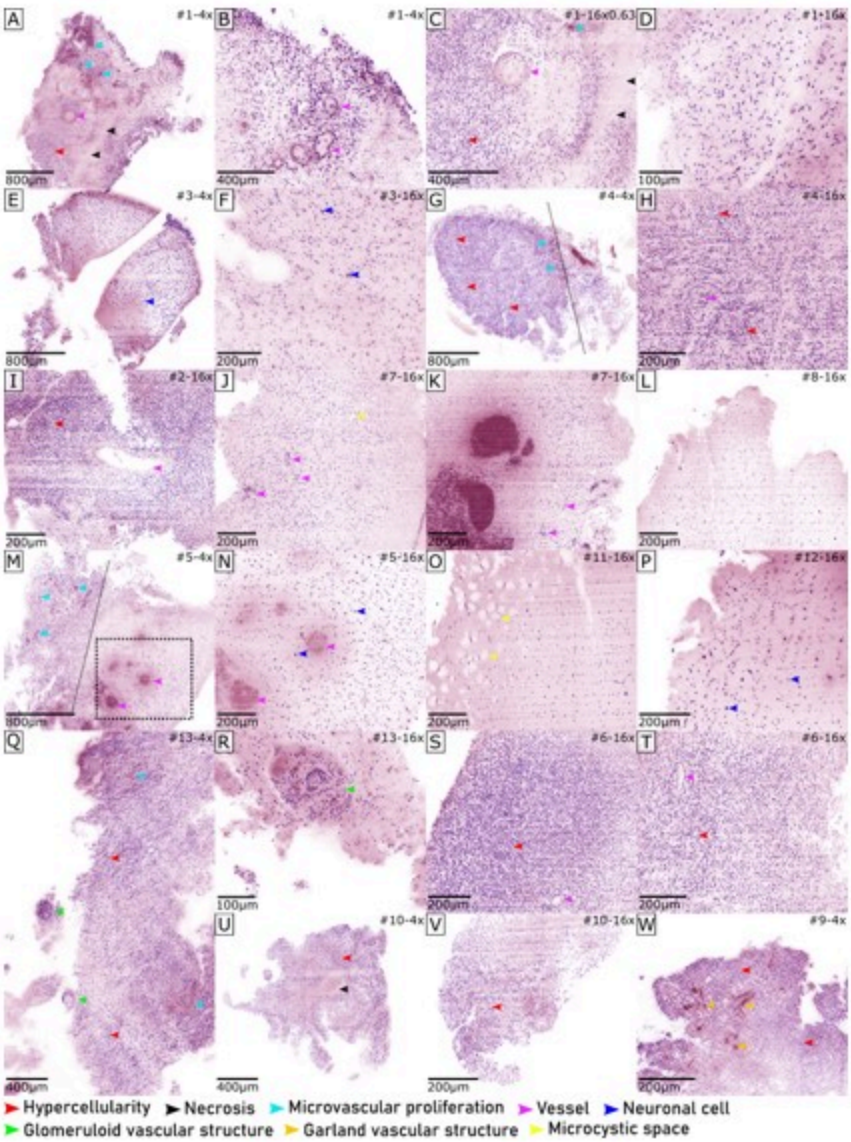

Figure 2

Application of pathoDISCO-HE to human gliomas. pathoDISCO-HE was applied to residual specimens from patients previously histologically diagnosed with grade 2-4 gliomas. Virtual H&E visualisation allowed identification of many characteristic features of glioblastoma such as hypercellularity, necrosis and microcysts. Various vasculature signatures could also be observed including microvascular proliferation and glomeruloid and garland-like vascular structures. Cells of neuronal morphology could be observed in some specimens. One specimen exhibited characteristic spindle cell morphology (**H**). Dashed lines in **G+M**indicate clear demarcation of high and low density areas at the infiltrating edge. Specimen number and magnification indicated in top right of each image.

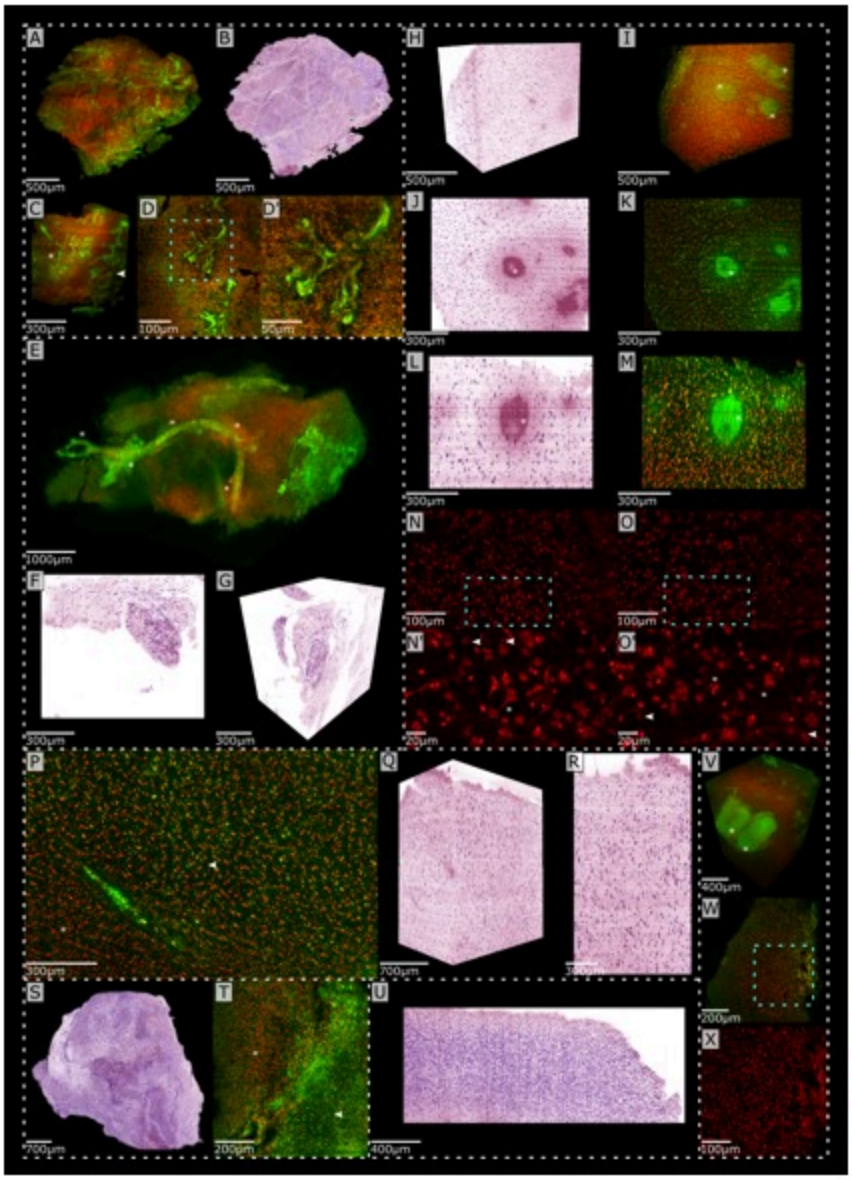

Figure 3

Volumetric histopathology of human gliomas. 3D visualisation of light sheet data allowed viewing of specimens from any angle and at any depth. Data was loaded either as virtual HE processed images or by assigning red and green colourmaps to greyscale images of cresyl violet and autofluorescence channels respectively and visualising by maximum intensity projection (MIP). **A-D:** Recurrent glioblastoma, specimen #9. **A+B:**visualisation of 4x magnification data by MIP and vHE respectively, autofluorescent vasculature structures can be observed throughout the specimen. **C:** MIP visualisation of 16x magnification data. Two distinct vascular signatures can be observed: vascular garlands (asterisk) and a considerably less dense vascular zone (arrowhead). **D:** 20µm slice exhibiting vascular garland and arrangement of local nuclei. **D':** Close-up of boxed area in **D**; elongated endothelial nuclei can be seen adjacent to autofluorescent vascular garland structures, further surrounded by dense tumour cell nuclei. **E-G:** Glioblastoma, specimen #13. **E:** MIP of 4x magnification data; a glomeruloid vessel can be traced over several millimetres (*). **F+G:** 2D and 3D Z-projections of glomeruloid vessel (*)

containing tissue, visualised by vHE (16x magnification). **H-O:** Recurrent glioblastoma, specimen #9, 16x magnification. Large vessels can be observed in the autofluorescence channel (*). **H+I:** 3D visualisation of vHE processed data and by MIP, identical perspective. **J-M:** Comparison of visualisation by vHE and MIP (20µm slice) in XY (**J+K**) and Z-projection (**L+M**). **N+O:** Zoomed in view of nuclear channel signal only. **N'+O':** Close-up of boxed regions in **N+O**. Various sub-cellular morphological elements can be observed including neurites (*) and chromatin (arrowheads). **P-R:** Glioblastoma, specimen #3 (16x magnification). **P:** 20µm MIP slice (XY) exhibiting discrete zones containing either cells of neuronal morphology (arrowhead) or small tumour cells (*). **Q+R:** 3D and 2D Z-projections of vHE processed stacks exhibiting primarily cells with neuronal morphology. **S+T:** Recurrent glioblastoma, specimen #1. **S:** 3D visualisation of vHE processed stack (4x magnification). **T:** 20µm slice (MIP) exhibiting starkly contrasting zones with high (*) and low (arrowhead) cell density. **U:** Glioblastoma, specimen #6. Z-projection of 16x magnification data exhibiting extremely high cell density and imaging to a depth of around 2200µm without loss of resolution. **V-X:** Recurrent glioblastoma, specimen #7. 16x magnification. **V:** 3D MIP exhibiting highly autofluorescent areas of bleeding. **W:**20µm MIP slice exhibiting small nucleated tumour cells. **X:** Close-up of boxed region in **W**, nuclear channel only.

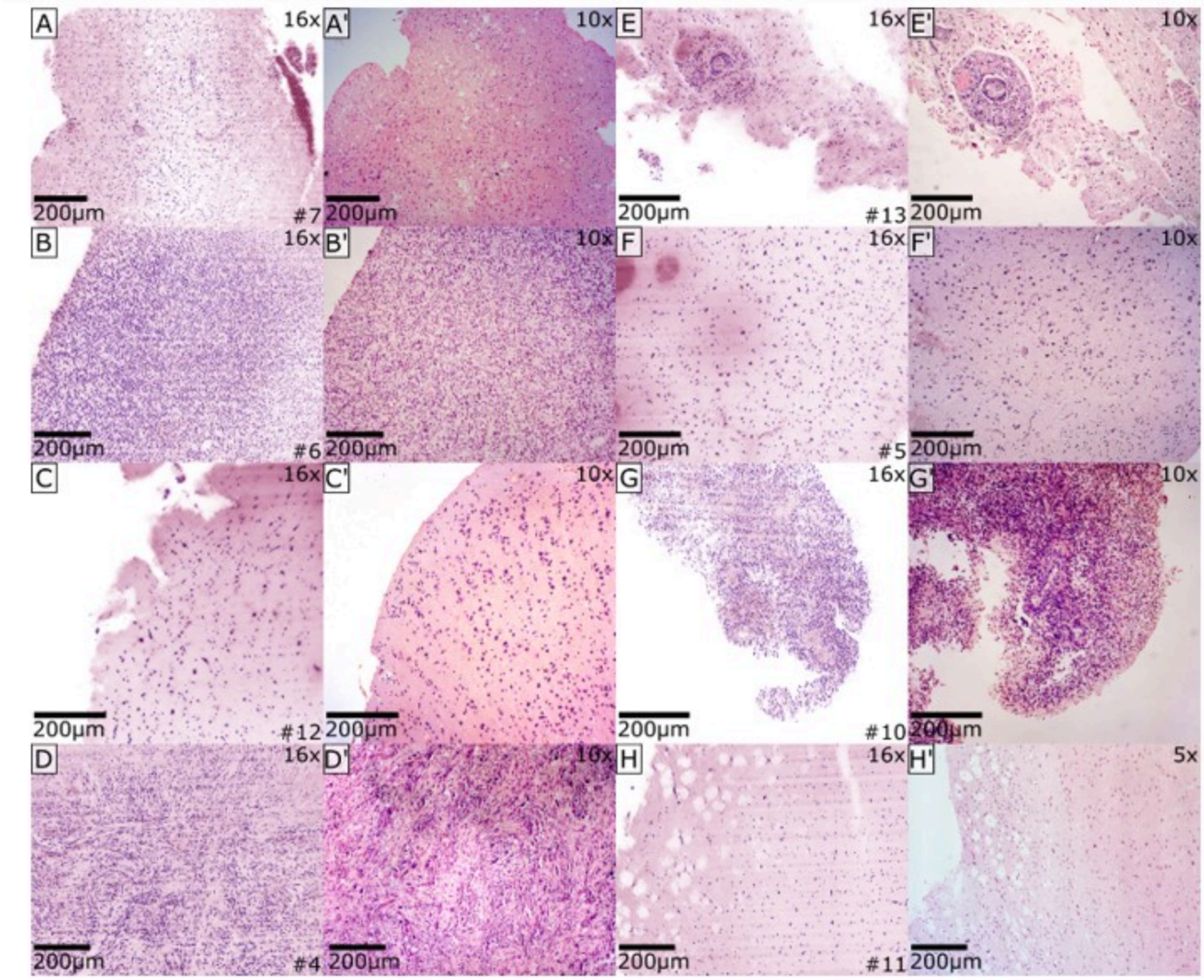

Figure 4

pathoDISCO-HE is reversible and recapitulates pathological features observed in standard histology. Following pathoDISCO-HE processing, specimens were re-processed using standard histopathology techniques to produce correlative H&E images. Comparable regions visualised with virtual H&E and standard H&E staining are displayed. Standard H&E images are marked with an apostrophe (‘). Magnification is indicated in the top right corner of each image. Specimen number is indicated in the bottom right corner of virtual H&E images. Further comparisons are provided in **Additional file 2**.

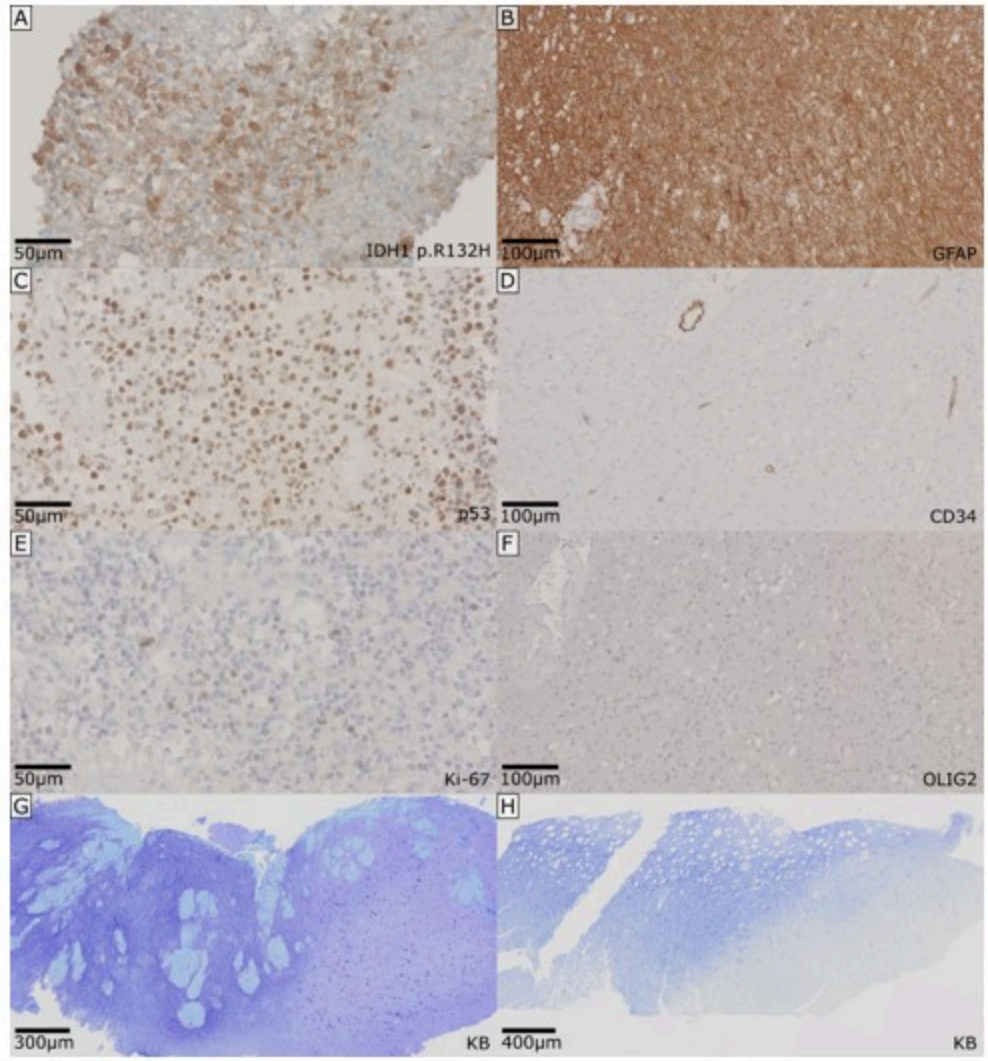

Figure 5

Compatibility of pathoDISCO-HE processed specimens with *post-hoc* immunolabelling and Klüver-Barrera staining. pathoDISCO-HE processed specimens were rehydrated, processed, sectioned at 5µm and labelled with a variety of glioma-relevant antibodies (**A-F**) or stained by the Klüver-Barrera method (**G+H**). **A,C,E**: Astrocytoma (grade 4, IDH-mutant) **B,D,F,G:** Glioblastoma. **H:** Astrocytoma (grade 2, IDH-mutant), with previous indications of subcortical medullary structure loss.

Supplementary Files

This is a list of supplementary files associated with this preprint. Click to download.

- Additionalfile1.pdf
- Video1.Sample1.mp4
- Video2.Sample3.mp4
- Video3.Sample5.mp4
- Video4.Sample9.mp4
- Video5.Sample13.mp4